

Spectroscopy of a fractional Josephson vortex molecule

U. Kienzle,^{1,*} J. M. Meckbach,² K. Buckenmaier,¹ T. Gaber,¹ H. Sickinger,¹
Ch. Kaiser,² K. Ilin,² M. Siegel,² D. Koelle,¹ R. Kleiner,¹ and E. Goldobin¹

¹*Physikalisches Institut – Center for Collective Quantum Phenomena and their Applications
in LISA+, Universität Tübingen, Auf der Morgenstelle 14, D-72076 Tübingen, Germany*

²*Institut für Mikro- und Nanoelektronische Systeme, Karlsruher
Institut für Technologie, Hertzstraße 16, D-76187 Karlsruhe, Germany*

(Dated: October 20, 2011)

In long Josephson junctions with multiple discontinuities of the Josephson phase, fractional vortex molecules are spontaneously formed. At each discontinuity point a fractional Josephson vortex carrying a magnetic flux $|\Phi| < \Phi_0$, $\Phi_0 \approx 2.07 \times 10^{-15}$ Wb being the magnetic flux quantum, is pinned. Each vortex has an oscillatory eigenmode with a frequency that depends on Φ/Φ_0 and lies inside the plasma gap. We experimentally investigate the dependence of the eigenfrequencies of a two-vortex molecule on the distance between the vortices, on their topological charge $\wp = 2\pi\Phi/\Phi_0$ and on the bias current γ applied to the Josephson junction. We find that with decreasing distance between vortices, a splitting of the eigenfrequencies occurs, that corresponds to the emergence of collective oscillatory modes of both vortices. We use a resonant microwave spectroscopy technique and find good agreement between experimental results and theoretical predictions.

PACS numbers: 74.50.+r, 85.25.Cp

Keywords: Annular long Josephson junction, sine-Gordon, fractional vortex, \wp -vortex, 0- κ -junction

I. INTRODUCTION

During the last decade the physics of fractional Josephson vortices has attracted a lot of attention.^{1–8} In contrast to the well known fluxons,⁹ fractional vortices carry the magnetic flux of $|\Phi| < \Phi_0$. Here we focus on the fractional vortices that emerge at the discontinuities of the Josephson phase^{10–12} in long Josephson junctions (LJJ) and disregard all other types, *e.g.*, splintered vortices.^{13–15} The phase discontinuity κ can be created by two tiny (compared to the Josephson penetration depth λ_J) current injectors,^{5,12,16} so that $\kappa \propto I_{\text{inj}}$, where I_{inj} is the current sent through the injectors.

A well known property of a long Josephson junction is the presence of a gap in the spectrum of electromagnetic waves (plasma waves) — the so-called plasma gap, which ranges from 0 to the plasma frequency ω_p . The value of $\omega_p \propto \sqrt{j_c}$ is $\sim 10 \dots 1000$ GHz, where j_c is the critical current density of the junction. In a LJJ with a fractional vortex pinned at the phase discontinuity, the vortex has an eigenfrequency ω_0 which is situated within the plasma gap (localized mode with a wave number $k = 0$). The value of $\omega_0(\wp, \gamma)$ depends on the topological charge \wp of the vortex and the normalized bias current γ applied to the LJJ.¹⁷

The topological charge of a single fractional vortex in an infinite LJJ with a κ discontinuity of the phase is defined as $\wp = \phi(+\infty) - \phi(-\infty) - \kappa$, where $\phi(x)$ is the Josephson phase, that is κ -discontinuous at one point. In simple words, \wp is a continuous advance of the phase when one goes from $x = -\infty$ to $x = +\infty$. Among all possible combinations of the phases at $x = \pm\infty$ only two irreducible combinations are stable¹⁸: the direct vortex with $\wp = -\kappa$ and a complementary vortex with $\wp = -\kappa + 2\pi \text{sgn}(\kappa)$. We assume that $|\kappa| \leq 2\pi$, otherwise the

structure either cannot be constructed (not a solution of the sine-Gordon equation) or is unstable — it splits into one or several fluxons and a fractional vortex with $|\wp| \leq 2\pi$.¹⁸ For $\wp \rightarrow 0$ there is a smooth transition to the flat phase state $\phi(x) = 0$ of the LJJ, while for $|\wp| \rightarrow 2\pi$ a(n) (anti)fluxon is formed. In contrast to the fractional vortex this fluxon is not pinned anymore and can move freely.⁹

The eigenfrequency of a single fractional vortex as a function of \wp and γ was already measured experimentally^{7,19} using microwave spectroscopy. Good agreement with numerical calculations was found.

Nowadays more complex fractional vortex systems, *e.g.* fractional vortex molecules consisting of two, three, *etc.* vortices can be created and studied experimentally.⁸ In particular, two-vortex molecules with degenerate ground states¹⁸ are proposed as a candidate for a macroscopic qubit.²⁰ In such a molecule, the coupling between vortices results in shifting/splitting of their eigenfrequency,¹⁷ very similar to the splitting of electronic energy levels in a real molecule when it is formed from atoms.

In this paper we experimentally investigate the eigenfrequencies in two types of symmetric two-vortex molecules: one with parallel (ferromagnetic) configuration and the topological charges (\wp, \wp) and one with antiparallel (antiferromagnetic) order and the topological charges $(\wp, -\wp)$. We use a spectroscopic measurement technique⁷ to determine the eigenmodes of the molecule as a function of applied bias current and topological charges.

The paper is organized as follows. In Sec. II we present the underlying theory and present numerically calculated ground states of molecules as well as their eigenfrequencies. Experimental results are presented and discussed in Sec. III. Section IV concludes the work.

II. THEORY

The perturbed sine-Gordon equation, which describes the dynamics of the Josephson phase is given by¹²

$$\phi_{xx} - \phi_{tt} - \sin(\phi) = \alpha\phi_t - \gamma(x) + \theta_{xx}(x), \quad (1)$$

where subscripts x and t denote derivatives with respect to space and time and the step function $\theta(x)$ describes the position of discontinuities. In the case of one κ discontinuity located at $x = 0$, $\theta(x) = \kappa H(x)$, where $H(x)$ is a Heaviside step function. In Eq. (1) the coordinate x and time t are normalized to the Josephson penetration depth λ_J and the inverse plasma frequency ω_p^{-1} , respectively. $\alpha = 1/\sqrt{\beta_c}$ is the dimensionless damping parameter, β_c is the Stewart-McCumber parameter. The bias current density γ is normalized to the critical current density j_c of the junction. To solve Eq. (1) numerically we introduce a new continuous phase¹² $\mu(x, t) = \phi(x, t) - \theta(x)$ and solve the resulting *smooth* equation for $\mu(x, t)$.

The eigenfrequency of a single vortex with a topological charge \wp in an unbiased ($\gamma = 0$) infinite LJJ without damping ($\alpha = 0$) is given by¹⁷

$$\omega_0(\wp) = \omega_p \sqrt{\frac{1}{2} \cos \frac{\wp}{4} \left(\cos \frac{\wp}{4} + \sqrt{4 - 3 \cos^2 \frac{\wp}{4}} \right)}. \quad (2)$$

In case of $\gamma \neq 0$ no analytical expression has been found and therefore the eigenfrequency has to be calculated numerically. A good approximation to the numerical results is given by

$$\omega_0(\wp, \gamma) \simeq \omega_0(\wp, 0) \cdot \sqrt[4]{1 - \left(\frac{\gamma}{\gamma_c} \right)^2}, \quad (3)$$

where

$$\gamma_c(\wp) = \left| \frac{\sin(\wp/2)}{\wp/2} \right|, \quad |\wp| \leq 2\pi \quad (4)$$

is the depinning current^{21,22} of the vortex. For bias currents exceeding γ_c , the fractional vortex flips into its complementary partner, thereby emitting a fluxon.

If one considers two discontinuities with the same absolute value of $|\kappa|$ that are situated at $x_{1,2} = \pm a/2$ (a is the distance between the discontinuities) in an infinite LJJ, four irreducible vortex configurations are possible.¹⁸ In the case of equal discontinuities, *i.e.* $(-\kappa, -\kappa)$, there exists the symmetric parallel (ferromagnetically) ordered (FM) vortex molecule with $(\wp_1, \wp_2) = (+\kappa, +\kappa)$ and the asymmetric antiparallel (antiferromagnetically) ordered (AFM) vortex molecule with $(\wp_1, \wp_2) = (+\kappa, +\kappa - 2\pi)$. For discontinuities of different signs, *i.e.* $(+\kappa, -\kappa)$, one gets either the symmetric antiparallel molecule with $(\wp_1, \wp_2) = (-\kappa, +\kappa)$ or the asymmetric parallel vortex molecule with $(\wp_1, \wp_2) = (-\kappa + 2\pi, +\kappa)$.

In the experiments described below we use annular LJJ^s²³ with two discontinuities at a distance $a = l/2$

from each other, where $l = 2\pi R/\lambda_J$ is the mean circumference of the junction normalized to λ_J . There are certain advantages of this particular geometry. First, due to a particular shape of the electrodes, annular junctions have intrinsically a much more homogeneous bias current density than linear LJJ^s,²⁴ which is important to measure $\omega_0(\gamma)$. Second, any real LJJ has a finite length, which results in a somewhat modified phase profile and eigenfrequency spectrum of the vortex molecules. The boundary conditions of the junction thereby impose an additional level of symmetry/ordering on the molecule. In an annulus this additional symmetry is always the same as the internal configuration of the molecule, FM or AFM.³⁹

In an annular junction each vortex has the same neighbor on both sides (right and left) so that magnetic field profiles and eigenfrequencies are somewhat different from the results obtained earlier for an infinite LJJ.¹⁸ This is especially true for short JJ^s. In principle, there are many eigenmodes $\omega_0 < \omega_1 < \dots$ enumerated according to their frequency. In the following we use ω_+ to denote the eigenfrequency of the vortex in-phase oscillations, while ω_- denotes the oscillation mode with a phase shift of π . They correspond to the two lowest eigenmodes ω_0 and ω_1 , *i.e.* $\omega_{\pm} = \omega_0$ or ω_1 . Depending on the configuration of the molecule ω_+ can be larger or smaller than ω_- . In general, the eigenfrequencies of a molecule can only be calculated numerically.²⁵ Due to the vast number of possible molecule configurations we, in the following, limit ourselves to the *symmetric* configurations and discuss them in more detail.

A. Parallel (FM) molecule

The magnetic field $\propto \mu_x(x)$ of a molecule consisting of two parallel ordered vortices pinned at $(-\kappa, -\kappa)$ discontinuities is exemplarily shown in Fig. 1(a) for an annular LJJ of length $l = 6$. The vortex distance is half of the junction length. No bias current is applied. Then, the FM configuration is stable for $|\kappa| < 2\pi$ and for all lengths due to annular boundary conditions and $a = l/2$, *cf.* Refs. 17 and 18 for more general cases. For $|\kappa| \geq 2\pi$, a single direct vortex with $|\wp| \geq 2\pi$ is not stable anymore. Instead, at each discontinuity a(n) (anti)fluxon and a $(\kappa - 2\pi \operatorname{sgn}(\kappa))$ -vortex (all of the same polarity)¹⁸ is formed.

The eigenfrequencies ω_{\pm} of a FM ordered molecule are shown in Fig. 2(a) as a function of κ for different vortex distances. Here, $\omega_+ < \omega_-$. The dependence of $\omega_{\pm}(a)$ is shown in Fig. 3 for two molecules with specific values of the discontinuities $\kappa_i = \kappa$. For comparison, the eigenfrequency of a single vortex in an *infinitely* long JJ is also shown. As can be seen the frequency splitting increases for smaller a (larger coupling). However, the divergence of the out-of-phase mode $\omega_- = \omega_1$ for $a \rightarrow 0$ is exclusively related to the fact, that also $l = 2a \rightarrow 0$ and therefore $\omega_1 \propto 1/l \rightarrow \infty$ for $l \ll 1$.

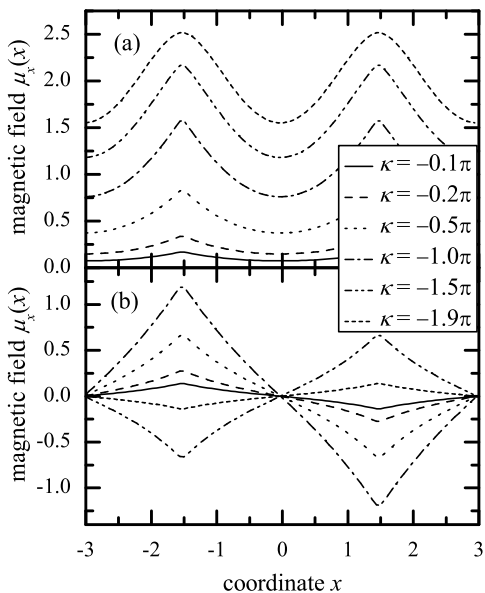


FIG. 1: Magnetic field profile $\mu_x(x)$ in an annular LJJ of length $l = 6$ and $a = 3$ for different values of κ : (a) parallel configuration, (b) antiparallel configuration.

B. Antiparallel (AFM) molecule

Figure 1(b) shows the magnetic field $\propto \mu_x(x)$ for the antiparallel molecule pinned at $(-\kappa, +\kappa)$ discontinuities in an annular LJJ of $l = 6$. In contrast to the parallel configuration there exists a critical value κ_c ($\pi < \kappa_c < 2\pi$), above which the vortices are not stable anymore: after exchanging one Φ_0 the $(+\kappa, -\kappa)$ -molecule turns into a complementary one $(+\kappa - 2\pi, -\kappa + 2\pi)$. The value of κ_c depends on a and can in general only be calculated numerically. For an AFM molecule in an infinitely long JJ κ_c was calculated in Ref. 18. Note that for $(2\pi - \kappa_c) < |\kappa| < \kappa_c$ both states $(+\kappa, -\kappa)$ and $(+\kappa - 2\pi, -\kappa + 2\pi)$ are stable and that for $\kappa \neq \pi$ these solutions have different energies.

The eigenfrequencies $\omega_{\pm}(\kappa)$ of the two lowest modes of the antiparallel configuration are shown in Fig. 2(b). The vertical lines describe the critical discontinuity κ_c for different vortex distances a . In contrast to the parallel configuration, here $\omega_+ > \omega_-$.

The dependence of the eigenfrequencies of two antiparallel vortices for fixed κ values as a function of the distance a is shown in Fig. 3. As with the parallel configuration the frequency splitting increases when a decreases. One has to recognize, that for $\kappa = 1.2\pi$ the critical vortex distance is $a_c \approx 2.15$. Therefore, the vortex state $(+\kappa, -\kappa)$ becomes unstable at $a \rightarrow a_c$ and the frequency $\omega_- = \omega_0 \rightarrow 0$. For $a < a_c$, ω_{\pm} correspond to the complementary state $(\kappa - 2\pi, 2\pi - \kappa)$, which is stable for all a . In comparison to the lowest eigenfrequency of the parallel configuration, this mode has a smaller frequency and this difference increases as $a \rightarrow 0$.

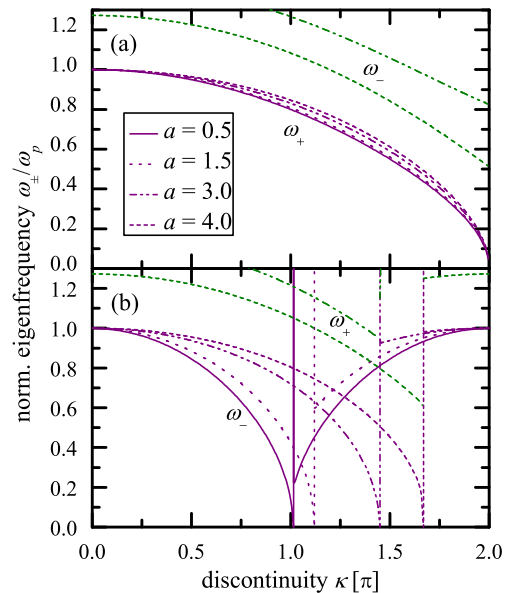


FIG. 2: (Color online) Numerically calculated lowest eigenmode(s) of a fractional vortex molecule in an annular LJJ for different distances a between the vortices: (a) parallel configuration, (b) antiparallel configuration. The junction length l is twice the distance a .

For a biased molecule ($\gamma \neq 0$) the approximation (3) can also be used to estimate $\omega_{\pm}(\varphi, \gamma)$.

III. EXPERIMENTS

For experiments we used underdamped long Nb-AlO_x-Nb annular tunnel junctions fabricated using standard trilayer technology.²⁶ Each JJ was equipped with two pairs of current injectors as shown in Fig. 4. Note that injector pairs are placed opposite to each other and directly on top/below the bias electrodes of the junction, as earlier measurements showed this layout to give best agreement of the critical current dependence $I_c(I_{inj})$ with theory, *i.e.* Eq. (4). As the JJs have been fabricated in an overlap geometry, their static and dynamic properties are modified by the overlap region of top and bottom electrode, the so-called idle region.^{27–32} Idle region effects can be taken into account by a renormalization of the junction length, *i.e.* by introducing an effective Josephson penetration depth $\lambda_{J,eff} > \lambda_J$. However, we find that the usual correction²⁹ overestimates the idle region effect. Table I summarizes the properties of the measured junctions, listing Josephson penetration depths and normalized junction lengths, with and without idle region corrections, as well as the normalized lengths we found to give best agreement with theory.

The measurements shown in this paper have been performed at $T = 4.2$ K with the resonant vortex excitation technique already used to determine the eigenfrequency

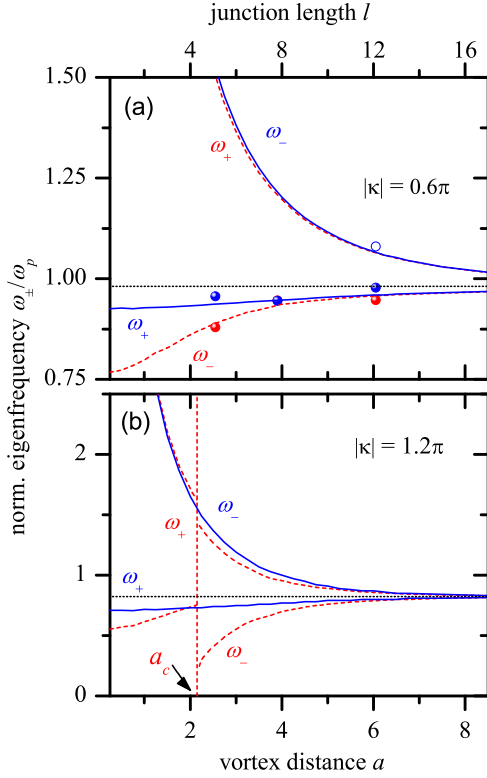


FIG. 3: (Color online) The two lowest eigenfrequencies $\omega_{\pm}(\kappa)$ of a symmetric vortex molecule in an annular LJJ with length $l = 2a$ for different distances a between the vortices: (a) $|\kappa| = 0.6\pi$ and (b) $|\kappa| = 1.2\pi$. Solid (dashed) lines correspond to the FM (AFM) configuration. For comparison the eigenfrequency of a single vortex in an *infinitely* long JJ is also shown (dotted lines). Full (open) symbols correspond to fitted values of ω_0 (ω_1) from experimental data, see text.

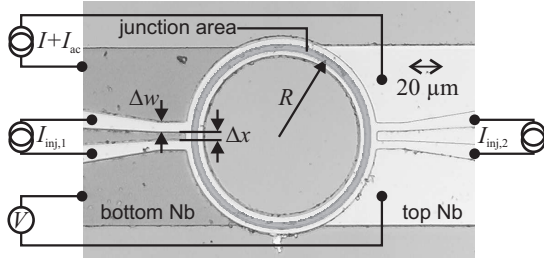


FIG. 4: Optical image (top view) of sample 2: annular LJJ with two pairs of injectors. The dc bias I is superimposed with a microwave induced ac current I_{ac} , that is capacitively coupled into the bias leads. $I_{inj,1}$ is applied to the left (top) pair of injectors, $I_{inj,2}$ to the right (bottom) pair respectively.

of a single fractional vortex.⁷ In brief, we continuously apply microwaves with fixed frequency $\omega_{ext} < \omega_0(\varphi)$ and fixed power to the junction while ramping up the bias current γ . As $\omega_i(\varphi, \gamma)$ decreases with increasing γ , cf. Eq. (3), the resonance condition $\omega_0(\varphi, \gamma_r) \simeq \omega_{ext}$ is achieved for some γ_r . Then, depending on applied mi-

#	R [μm]	j_c [A/cm ²]	λ_J [μm]	l_b	$\lambda_{J,eff}$ [μm]	l_{eff}	l	$\omega_p/2\pi$ [GHz]
1	30	112	35.7	5.3	41.4	4.6	5.1	45.1
2	50	90	39.8	7.9	46.1	6.8	7.8	44
3	80	77	40.9	12.3	43.7	11.4	12.1	36

TABLE I: Sample properties measured at $T = 4.2$ K. Junction widths w and injector distances Δx are $5 \mu\text{m}$, injector widths Δw are $5 \mu\text{m}$, except for sample 3, where $\Delta w = 2 \mu\text{m}$. $l_{eff} = 2\pi R/\lambda_{J,eff}$ and $l_b = 2\pi R/\lambda_J$ are the normalized junction length with and without idle region corrections and R is the radius of the junction. l is the length which gives best agreement between measurement and theory. ω_p is the plasma frequency obtained from spectroscopic measurements.

crowave power and the internal damping of the junction, the vortex molecule may flip and switch the junction into its resistive state.³³ If, however, the junction remains in the zero-voltage state it switches to the non-zero voltage state by means of thermal escape when the bias approaches the fluctuation-free critical current γ_c . By repeatedly measuring the switching current and systematically scanning microwave power and frequency we can map out the resonances corresponding to the eigenmodes of the molecule. As the JJ itself is a non-linear oscillator, resonances shift towards lower frequencies with increasing microwave power.^{9,33–36} This is especially relevant at small γ where the energy barrier between the zero and the non-zero voltage state is still large and high microwave power is necessary for switching. We therefore determine γ_r from the measurements with the lowest power to keep non-linear effects to a minimum.

Before spectroscopy was performed, injectors were calibrated. For this we first measured the critical current I_c of the junction as a function of the current through each injector pair $I_{inj,1}$ and $I_{inj,2}$ individually. From Eq. (4) and $\kappa \propto I_{inj}$ we then determined the injector currents $I_{inj,i}^{min}$ necessary to create a discontinuity of $\kappa_i = 2\pi$, where $I_c(I_{inj,i})$ have the cusp like first minima. Figure 5(a) and (b) show the measured $I_c(I_{inj,i})$ dependences of sample 1, as well as the fitted theoretical curves. Although both injector pairs have nominally the same width and distance, the $I_{inj,i}^{min}$ are usually somewhat different. In sample 3 the inequality was introduced intentionally, as we deliberately cut the top wiring layer between the injectors to increase the coupling of $I_{inj,1}$ to the junction. However, in samples 1 and 2, both injector pairs are identical by design. Here, we believe, the deviations are due to lithographical inaccuracy and different thicknesses of the top and bottom Nb layer. To create *symmetric* vortex molecules we henceforth applied the injector currents $I_{inj,i} = \pm \kappa |I_{inj,i}^{min}|/2\pi$ simultaneously.

Figure 5(c) shows the measured and the numerically calculated $\gamma_c = I_c(\kappa)/I_c(0)$ dependence of a symmetric FM vortex molecule pinned at (κ, κ) discontinuities. As can be seen there is a good agreement between experiment and theory. Note that $\gamma_c(+\kappa, +\kappa)$ looks qualitatively similar to $\gamma_c(\kappa)$ for a single vortex,²¹ yet the first

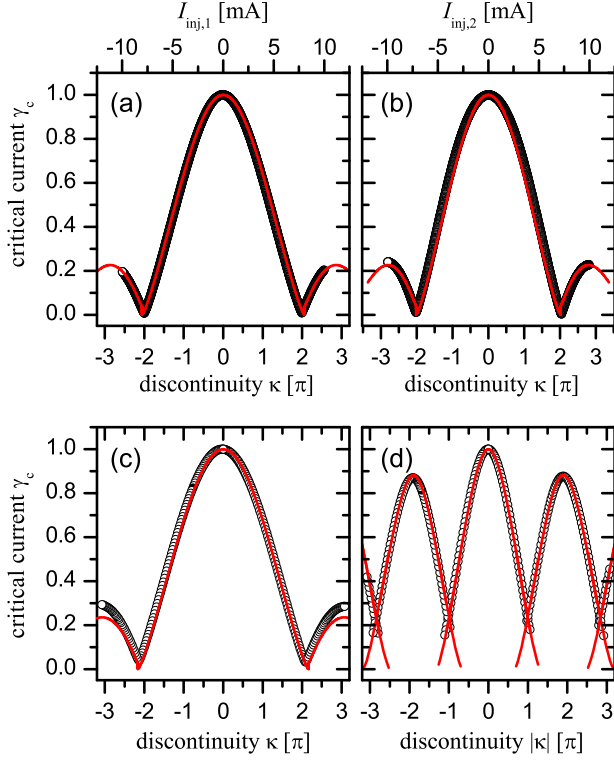


FIG. 5: (Color online) Measured (symbols) and numerically calculated (red line) critical current $\gamma_c = I_c(I_{\text{inj},i})/I_c(0)$ as a function of injector current. Single vortex cases with either (a) injector current $I_{\text{inj},1}$ or (b) $I_{\text{inj},2}$ applied. (c) FM and (d) AFM molecule cases corresponding to $(+\kappa, +\kappa)$ and $(+\kappa, -\kappa)$ discontinuities. Data is shown for sample 1. For the vortex molecule injector currents $I_{\text{inj},i} = \pm\kappa|I_{\text{inj},i}^{\text{min}}|/2\pi$ were applied simultaneously.

minimum positions are slightly different: γ_c^{min} of a symmetric FM vortex molecule in an annular JJ with a *finite* width Δx , Δw of injector pairs corresponds to a κ_i value, which is slightly larger than 2π .

The $\gamma_c(+\kappa, -\kappa)$ curve for the AFM molecule is depicted in Fig. 5(d). Again, experimental data and numerical calculations are in good agreement. In contrast to the FM configuration, here the γ_c -minima correspond to $|\kappa| \simeq (2n+1)\pi$ instead of $\kappa \simeq 2n\pi$, cf. Eq. (4). Note that the $\gamma_c(+\kappa, -\kappa)$ curve is identical to the $\gamma_c(\kappa)$ dependence of a *linear* LJJ of length $l/2$ with a *single* central vortex.³⁷ As already mentioned in Sec. II B, the AFM molecule exhibits regions of bistability of the direct and the complementary vortex states around $|\kappa| = (2n+1)\pi$. Between $2\pi - \kappa_c(a) < \kappa < \kappa_c(a)$ the critical current of both vortex states can be traced out,⁸ see Fig. 5(d). In AFM configuration the $\gamma_c(+\kappa, -\kappa)$ pattern sensitively depends on junction length as well as on injector size³⁷: For infinitesimally small injectors, the $\gamma_c(+\kappa, -\kappa)$ is 2π periodic with maxima at $\kappa = 2\pi n$ and minima at $\kappa = (2n+1)\pi$. For finite size injectors, however, this is not the case: $\gamma_c(\pm 2\pi n, \mp 2\pi n) < \gamma_c(0, 0)$ and the minimum positions shift to $\kappa > (2n+1)\pi$. In the FM

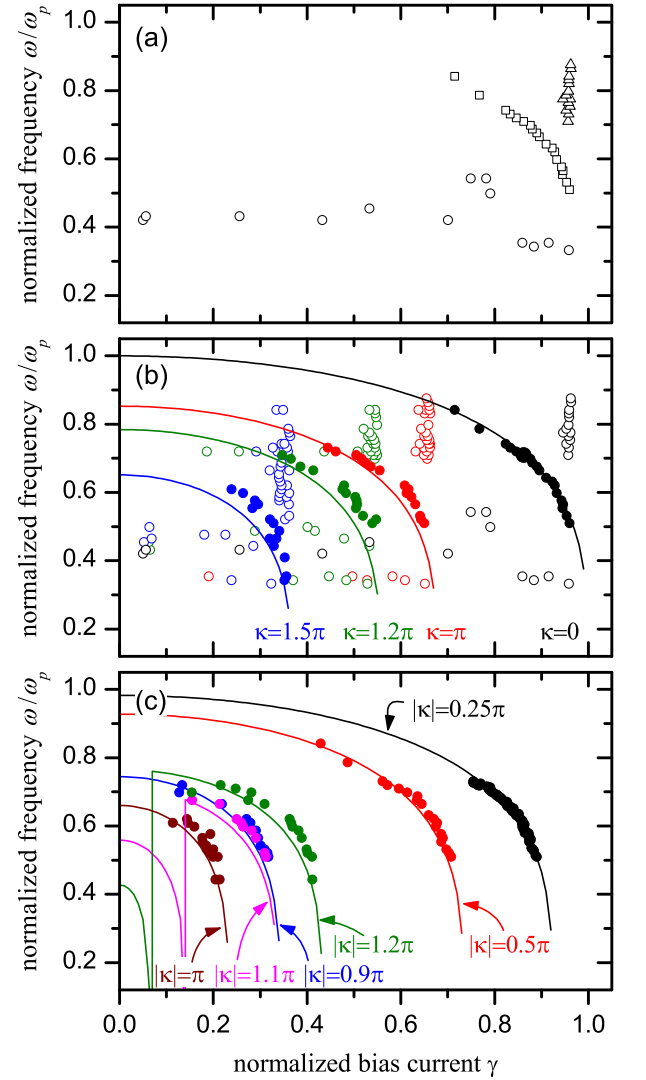


FIG. 6: (Color online) Comparison of measured resonance peak positions (symbols) with the numerically calculated $\omega_0(\kappa, \gamma)$ dependences (solid lines). Data is shown for (a) the plasma frequency scan ($\kappa = 0$), (b) the FM $(-\kappa, -\kappa)$ and (c) the AFM $(-\kappa, +\kappa)$ molecule configurations in sample 1. Symbols of same color correspond to the same κ value. Symbols are explained in the text.

case basically only $I_{\text{inj},i}^{\text{min}}$ depends on injector size — the shape of the curve does not change. By carefully comparing the $I_c(I_{\text{inj},i})/I_c(0)$ curves of the AFM configuration with numerical simulations we obtained the normalized junction length l , see Tab. I, which we used for the subsequent calculation of eigenfrequencies.

After calibration of injectors we spectroscopically mapped out the well-known dependence of the plasma frequency $\omega_0(0, \gamma) = \omega_p \sqrt{1 - \gamma^2}$ on applied bias current. Figure 6(a) shows exemplarily the results of the plasma frequency scan of sample 1. All measured resonance peak positions are plotted. Beside the desired

plasma resonance (squares), additional resonances were observed. They do not correspond to a sub- or a superharmonic excitation of the plasma resonance, but can be subsumed into two groups. One set of resonances (triangles) occurs at high frequencies and close to the critical current γ_c of the junction. These resonances are most likely the result of a microwave enhanced thermal escape. The second group of resonances (circles) seem to be erratically distributed over the full bias current range. Yet, a comparison with other spectroscopic measurements, *e.g.* see Fig. 6(b), shows that they appear in rather small frequency bands, where the coupling of the microwave current to the junction is exceptionally high. We therefore believe that they are the result of a parasitic coupling of the junction to cavity modes of the sample box and the bias circuitry. Note, that in contrast to a typical spectroscopic measurement of the plasma frequency or the eigenfrequency of a single fractional vortex, *e.g.* see Ref. 7, we did not simply trace out the desired resonance curve by optimizing the measured frequency range and the applied microwave power. Instead, we systematically scanned over a large microwave power and frequency range to ensure, that no resonance is missed. Evidently, this measurement technique also reveals parasitic resonances, which are not of interest and must be removed in a manual post-selection process. From the measured plasma resonance (squares) we extracted ω_p and the fluctuation-free critical current $I_0 = j_c 2\pi R w$ of the junction, which then served as a reference for the following measurements on vortex molecules. R is the junction radius, w the junction width. We also determined ω_p from measurements of the zero field steps³⁸ on the current-voltage characteristics of the junction. After corrections due to idle region effects^{28,30,31} we typically find both values in agreement by better than 90%.

Figure 6(b) shows all measured resonance peak positions of a set of FM ordered vortex molecules in sample 1. Also plotted are the corresponding numerically calculated $\omega_0(\kappa, \gamma)$ dependences. As sample 1 is rather short ($l = 5.1$), $\omega_1 = \omega_-$ is much larger than the highest frequency of our rf-generator and could therefore not be measured. As already discussed for the plasma frequency measurement, we partitioned the data — eigenmode resonances are plotted with full symbols, whereas open symbols correspond to parasitic resonances. Beside a certain ambiguity of the data selection process, a good agreement with theory can clearly be seen.

The measurement results of the more interesting AFM case are shown in Fig. 6(c). Here, injector currents were reset after each switching current measurement to ensure a well defined initial molecule state. Also, only eigenmode resonances are plotted. Again, there is a good agreement between experiment and theory. It is interesting to note, that for $\kappa > \pi$ almost no signature of the direct vortex state $(-\kappa, \kappa)$ can be seen. Instead, the measured resonances correspond to the complementary state $(2\pi - \kappa, \kappa - 2\pi)$, which has a higher eigenfrequency ω_0 . As mentioned in Sec. II B, for $\pi < \kappa < \kappa_c$ both the

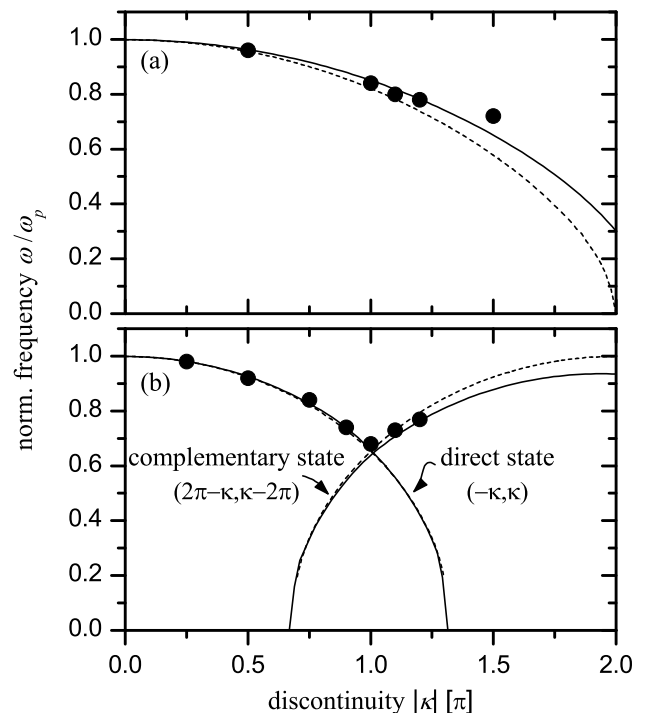


FIG. 7: Comparison of extrapolated zero bias eigenfrequency (symbols) with the numerically calculated $\omega_0(\kappa, \gamma = 0)$ dependence (lines) of a vortex molecule in sample 1. (a) FM order, (b) AFM order. Dashed lines correspond to ideal discontinuities, whereas solid lines take the finite injector size into account.

direct and the complementary molecule state are stable, yet have different energies and different critical currents, *cf.* Fig. 5(d). In case of sample 1, $\kappa_c \simeq 1.3\pi$. When a bias current is applied that exceeds γ_c of the direct state, the molecule flips into the complementary state by exchange of one fluxon between the vortices. In contrast to the FM case however, here this transition is not automatically followed by the switching of the junction into a non-zero voltage state. So, as the experimental data indicates, already for $\kappa = 1.1\pi$ the vortex flipping usually remains undetected and only the more stable complementary state is measured.

Using Eq. (3) we fitted the measured resonance peaks (full symbols) in Fig. 6 leaving $\gamma_c(\kappa)$ and $\omega_0(\kappa)$ at zero bias as free parameters. Figure 7 shows the obtained values of $\omega_0(\kappa)$ and compares them with theory. As expected from Fig. 6 we find very good agreement. As the finite injector size influences the eigenfrequency spectrum, Fig. 7 also shows the theoretical dependences of $\omega_0(\kappa)$ for ideal discontinuities. Clearly, only for large discontinuities, *i.e.* $\kappa \gtrsim \pi$, differences become significant.

In sample 1 only the lowest eigenmode could be investigated due to limitations of our rf-generator. To experimentally investigate higher eigenmodes we measured sample 3, which is the longest JJ and also has the lowest plasma frequency. Figures 8(a) and (b) show the ob-

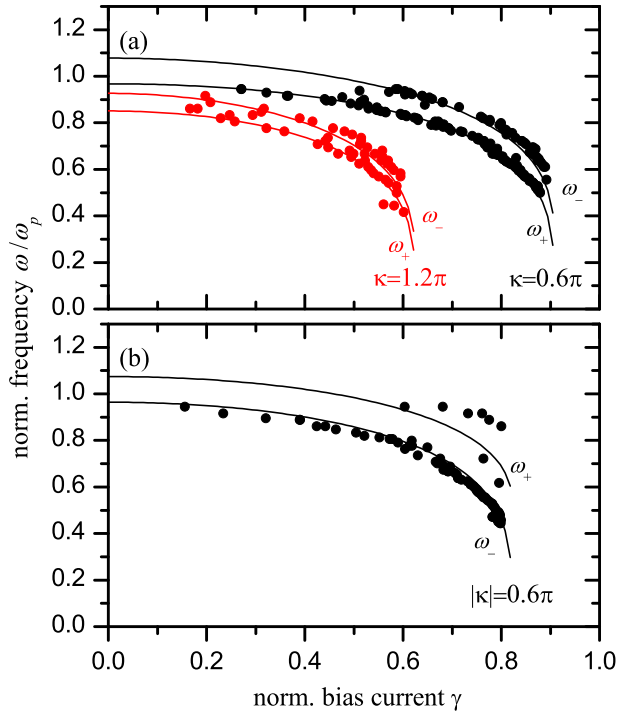


FIG. 8: (Color online) Comparison of measured resonance peak positions (symbols) with the numerically calculated $\omega_{\pm}(\kappa, \gamma)$ dependences (solid lines). Data is shown for (a) FM and (b) AFM molecule configurations in sample 3. Same colors correspond to the same κ value.

served resonance peak positions of the measured FM and AFM configurations. Parasitic resonances are not plotted. Interestingly, in the FM configuration both eigenmodes ω_{\pm} can clearly be seen, yet only the lowest mode is present in the AFM state. Further measurements confirmed, that for all symmetric FM states we selected, the observed resonances clearly showed two modes coinciding with the theoretical dependence of ω_{\pm} , yet only a single mode for the AFM states. Even more surprising, measurements on two other samples of proper length (not shown) revealed no trace of ω_1 , neither in AFM nor the FM state, indicating some general problem with the excitation of higher modes — sample 3 being the exception. So far it is unclear to us, whether this behavior is owed to the particular way we apply microwaves to the JJ, *i.e.* by capacitive coupling to the bias line, or to a more fundamental reason.

As has been shown in Fig. 3 coupling between the vortices in a molecule can be adjusted by changing the distance a between them — the smaller is the distance, the larger is the coupling (frequency splitting). Clearly, compared to the FM configuration, the deviation of the frequency of the lowest mode from the single vortex frequency (2) is much more pronounced in the AFM case. The configuration related, different dependence of ω_0 on a can also be seen in Fig. 9, where we directly

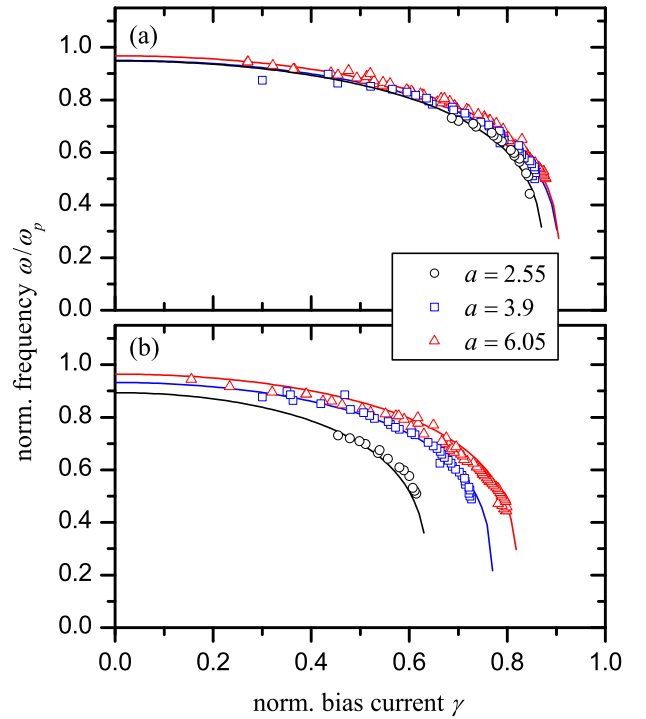


FIG. 9: (Color online) Comparison of the resonance peak positions of the lowest mode for annular LJJJs of different lengths with two fractional Josephson vortices: experiment (open symbols), numerical simulations (solid lines). (a) FM $(-0.6\pi, -0.6\pi)$ -molecule. (b) AFM $(-0.6\pi, +0.6\pi)$ -molecule.

compare $\omega_0(\gamma)$ of the FM and AFM ordered molecules $(\varphi_1, \varphi_2) = (-0.6\pi, -0.6\pi)$ and $(\varphi_1, \varphi_2) = (-0.6\pi, +0.6\pi)$ for three different vortex distances a . As expected, the eigenfrequency ω_0 of the AFM state is much more sensitive to a than of the FM state. Finally, we used Eq. (3) to obtain $\omega_{0,(1)}(\kappa)$ at $\gamma = 0$ from measurements, which are shown in Fig. 3.

IV. CONCLUSIONS

We experimentally investigated the interaction of fractional Josephson vortices in a symmetric two-vortex molecule by measuring the oscillatory eigenmodes of the molecule spectroscopically. We observe a splitting of the single vortex eigenmode due to vortex-vortex coupling. The emerging molecule modes correspond to an in-phase and an out-of-phase oscillation of the individual vortices. The measured dependence of the eigenfrequencies of the molecule on applied bias current, topological charge φ of the vortices and vortex ordering are in good agreement with numerical calculations. We find that with decreasing vortex distance coupling and frequency splitting increases. Depending on the configuration of the molecule, *i.e.* parallel or antiparallel vortex order, spectra show significantly different behavior, which can, in principle,

be used to identify an unknown vortex state.

Acknowledgments

This work was supported by the Deutsche Forschungsgemeinschaft via SFB/TRR-21 and the DFG Center of

Functional Nanostructures (project B1.5). U. K. gratefully acknowledges support by the Bischöfliche Studienförderung Cusanuswerk, K. B. and H. S. by the Evangelisches Studienwerk e.V. Villigst.

-
- * Electronic address: uta.kienzle@uni-tuebingen.de
- ¹ J. R. Kirtley, C. C. Tsuei, M. Rupp, J. Z. Sun, L. S. Yu-Jahnes, A. Gupta, M. B. Ketchen, K. A. Moler, and M. Bhushan, *Phys. Rev. Lett.* **76**, 1336 (1996).
 - ² J. R. Kirtley, C. C. Tsuei, and K. A. Moler, *Science* **285**, 1373 (1999).
 - ³ H.-J. H. Smilde, Ariando, D. H. A. Blank, G. J. Gertsma, H. Hilgenkamp, and H. Rogalla, *Phys. Rev. Lett.* **88**, 057004 (2002), .
 - ⁴ H. Hilgenkamp, Ariando, H.-J. H. Smilde, D. H. A. Blank, G. Rijnders, H. Rogalla, J. R. Kirtley, and C. C. Tsuei, *Nature* **422**, 50 (2003).
 - ⁵ E. Goldobin, A. Sterck, T. Gaber, D. Koelle, and R. Kleiner, *Phys. Rev. Lett.* **92**, 057005 (2004).
 - ⁶ M. Weides, M. Kemmler, H. Kohlstedt, R. Waser, D. Koelle, R. Kleiner, and E. Goldobin, *Phys. Rev. Lett.* **97**, 247001 (2006).
 - ⁷ K. Buckenmaier, T. Gaber, M. Siegel, D. Koelle, R. Kleiner, and E. Goldobin, *Phys. Rev. Lett.* **98**, 117006 (2007).
 - ⁸ A. Dewes, T. Gaber, D. Koelle, R. Kleiner, and E. Goldobin, *Phys. Rev. Lett.* **101**, 247001 (2008).
 - ⁹ K. K. Likharev, *Dynamics of Josephson Junctions and circuits* (Gordon and Breach Publishers, 1986).
 - ¹⁰ L. N. Bulaevskii, V. V. Kuzii, and A. A. Sobyenin, *Solid Stat. Comm.* **25**, 1053 (1978).
 - ¹¹ J. H. Xu, J. H. Miller, and C. S. Ting, *Phys. Rev. B* **51**, 11958 (1995).
 - ¹² E. Goldobin, D. Koelle, and R. Kleiner, *Phys. Rev. B* **66**, 100508 (2002).
 - ¹³ R. G. Mints, I. Papiashvili, J. R. Kirtley, H. Hilgenkamp, G. Hammerl, and J. Mannhart, *Phys. Rev. Lett.* **89**, 067004 (2002).
 - ¹⁴ A. Buzdin and A. E. Koshelev, *Phys. Rev. B* **67**, 220504 (2003).
 - ¹⁵ E. Goldobin, D. Koelle, R. Kleiner, and A. Buzdin, *Phys. Rev. B* **76**, 224523 (2007).
 - ¹⁶ A. V. Ustinov, *Appl. Phys. Lett.* **80**, 3153 (2002).
 - ¹⁷ E. Goldobin, H. Susanto, D. Koelle, R. Kleiner, and S. A. van Gils, *Phys. Rev. B* **71**, 104518 (2005).
 - ¹⁸ E. Goldobin, D. Koelle, and R. Kleiner, *Phys. Rev. B* **70**, 174519 (2004).
 - ¹⁹ T. Gaber, K. Buckenmaier, D. Koelle, R. Kleiner, and E. Goldobin, *Appl. Phys. A* **89**, 587 (2007).
 - ²⁰ E. Goldobin, K. Vogel, O. Crasser, R. Walser, W. P. Schleich, D. Koelle, and R. Kleiner, *Phys. Rev. B* **72**, 054527 (2005).
 - ²¹ B. A. Malomed and A. V. Ustinov, *Phys. Rev. B* **69**, 064502 (2004).
 - ²² E. Goldobin, N. Stefanakis, D. Koelle, and R. Kleiner, *Phys. Rev. B* **70**, 94520 (2004).
 - ²³ A. Davidson, B. Dueholm, B. Kryger, and N. F. Pedersen, *Phys. Rev. Lett.* **55**, 2059 (1985).
 - ²⁴ N. Martucciello, J. Mygind, V. P. Koshelets, A. V. Shchukin, L. V. Filippenko, and R. Monaco, *Phys. Rev. B* **57**, 5444 (1998).
 - ²⁵ E. Goldobin and A. Wallraff, *StkJJ — User's Reference*, <http://www.geocities.com/SiliconValley/Heights/7318/StkJJ.htm> (2006).
 - ²⁶ C. Kaiser, J. M. Meckbach, K. S. Ilin, J. Lisenfeld, R. Schäfer, A. V. Ustinov, and M. Siegel, *Supercond. Sci. Technol.* **24**, 035005 (2011).
 - ²⁷ J. G. Caputo, N. Flytzanis, and M. Devoret, *Phys. Rev. B* **50**, 6471 (1994).
 - ²⁸ J. G. Caputo, N. Flytzanis, and E. Vavalis, *Int. J. Mod. Phys. C* **7**, 191 (1996).
 - ²⁹ J. G. Caputo, N. Flytzanis, V. Kurin, N. Lazarides, and E. Vavalis, *J. Appl. Phys.* **85**, 7291 (1999).
 - ³⁰ G. Lee, *IEEE Trans. Appl. Supercond.* **1**, 121 (1991), ISSN 1051-8223.
 - ³¹ G. S. Lee and A. T. Barfknecht, *IEEE Trans. Appl. Supercond.* **2**, 67 (1992), ISSN 1051-8223.
 - ³² N. Flytzanis, N. Lazarides, A. Chiginev, V. Kurin, and J. G. Caputo, *J. Appl. Phys.* **88**, 4201 (2000).
 - ³³ M. V. Fistul and A. V. Ustinov, *Phys. Rev. B* **63**, 024508 (2000).
 - ³⁴ N. Grønbech-Jensen, M. G. Castellano, F. Chiarello, M. Cirillo, C. Cosmelli, L. V. Filippenko, R. Russo, and G. Torrioli, *Phys. Rev. Lett.* **93**, 107002 (2004).
 - ³⁵ N. Grønbech-Jensen and M. Cirillo, *Phys. Rev. B* **70**, 214507 (2004).
 - ³⁶ J. A. Blackburn, M. Cirillo, and N. Grønbech-Jensen, *Phys. Lett. A* **374**, 2827 (2010).
 - ³⁷ T. Gaber, E. Goldobin, A. Sterck, R. Kleiner, D. Koelle, M. Siegel, and M. Neuhaus, *Phys. Rev. B* **72**, 054522 (2005).
 - ³⁸ T. A. Fulton and R. C. Dynes, *Solid State Commun.* **12**, 57 (1973).
 - ³⁹ The phase profile of a two-vortex molecule in a finite LJJ can be constructed by employing vortex images using the boundaries of the junction as mirrors.⁵ In linear geometry the phase resembles a piece of length l of an infinite chain of AFM ordered vortex pairs, even for a FM ordered molecule. Annular geometry, however, results in a FM order of vortex pairs, thereby conserving the molecules inner configuration.